9

Control Strategies for Variable-speed Fixed-pitch Wind Turbines

Bunlung Neammanee, Somporn Sirisumrannukul and Somchai Chatratana[1]
Department of Electrical Engineering, Faculty of Engineering
King Mongkut's University of Technology North Bangkok
[1]National Science and Technology Development Agency
Thailand

1. Introduction

This chapter deals with a design of controllers for variable-speed fixed-pitch wind turbines. The chapter begins with an introduction to wind turbine control and the detail of nonlinear models of the wind energy conversion system (WECS). Linearization around a set of equilibrium points is presented to obtain a linear parameter variable model from a nonlinear system. Open-loop characteristics for small signals are then described to analyze dynamic behaviors under different operating conditions. The control objectives for variable-speed fixed-pitch wind turbines detailed in this chapter consists of three operating conditions:

1. Maximization of extracted energy: The wind turbine should extract wind energy at the highest efficiency to obtain the highest energy conversion ratio. Three alternative maximum peak power tracking (MPPT)-based algorithms for fixed pitch wind turbines are introduced. The first algorithm is guided by a torque reference (Mirecki et at., 2004). The second method searches an optimal operating point from the slope of the power-rotational speed curve. The last method is based on the control objective derived from a fuzzy rule base.
2. Limitation of extracted energy with active stall with rotational speed control: The aim of this control is to limit stresses on the turbine while minimizing the power fluctuations around a constant value, normally around the nominal power.
3. Control of MPPT and stall regulation at the overlapping region: This operating condition is effective with constant rotational speed control.

The controller objectives, controller schemes and controller designs are discussed in detail. The developed controllers for fixed-pitch wind turbines are based on a speed and torque-feedback control scheme. The proper design of the reference signal allows accurate tracking of each control strategy along the entire operating range. Hardware and software implementation for the control algorithms are explained. The case studies were carried out with two laboratory experiments with a developed wind turbine simulator: 1) three MPPT algorithms and active stall regulation with rotational speed control, and 2) an MPPT algorithm with a grid-connected converter. The chapter is concluded in the last section. The references are also provided for further research and studies.

Source: Wind Power, Book edited by: S. M. Muyeen,
ISBN 978-953-7619-81-7, pp. 558, June 2010, INTECH, Croatia, downloaded from SCIYO.COM

2. Model of variable speed fixed-pitch wind energy conversion system

2.1 Modeling of rotor blade characteristics

A wind speed generally varies with elevation of the blades (i.e., every single spot on the turbines may not have the same wind speed). Modeling wind speed taking into account all different positions on the blades could be, therefore, very difficult. For this reason, a single value of wind speed is normally applied to the whole wind turbines. Modeling the rotor blade characteristic requires the tip speed ratio (TSR) and the relationship of torque and power coefficient versus TSR. The TSR is obtained from

$$\lambda = \lambda(v_t, \omega_t) = \frac{\omega_t R}{v_t} \tag{1}$$

where λ = tip speed ratio [rad.s]
v_t = wind speed [m/s]
ω_t = rotational speed [rad/s]
R = blade radius [m]
The power captured by the blades, P_{turb}, can be calculated by

$$P_{turb} = \frac{\rho}{2}\pi R^2 v_t^3 C_P(v_t, \omega_t, \beta) \tag{2}$$

The aerodynamic torque acting on the blades, T_a, is obtained by

$$T_a = \frac{\rho}{2}\pi R^3 v_t^2 C_T(v_t, \omega_t, \beta) \tag{3}$$

where ρ = air density [kg/m^3]
C_P = power coefficient [-]
C_T = torque coefficient [-]
β = pitch angle [degree]
If C_P is known, the aerodynamic torque can also be calculated from

$$T_a = \frac{\rho}{2}\pi R^2 v_t^3 C_P(v_t, \omega_t, \beta)/\omega_t \tag{4}$$

It can be seen from the above two equations that C_T and C_P are a function of λ and β. In this chapter, β is kept constant; namely, the pitch angle is fixed and this is generally true for small and medium sized wind turbines. Therefore, C_T and C_P depend only upon λ.
Figure 1 shows a relationship of C_T versus TSR of a typical 3 kW, three blade horizontal axis wind turbine with a rotor diameter of 4.5 m (Kojabadi et at., 2004). This curve represents an important characteristic in determining the starting torque of the wind turbine. In general, this curve is available from the manufacture or obtained from a field test. With this curve, C_P, indicating the efficiency of power conversion of the rotor blades, can be calculated by multiplying C_T with λ. Figure 1 also shows the C_T-λ profile corresponding to the C_P-λ curve. It is important to note that the power and torque coefficient of a wind turbine depends on aerodynamic design of the blades.

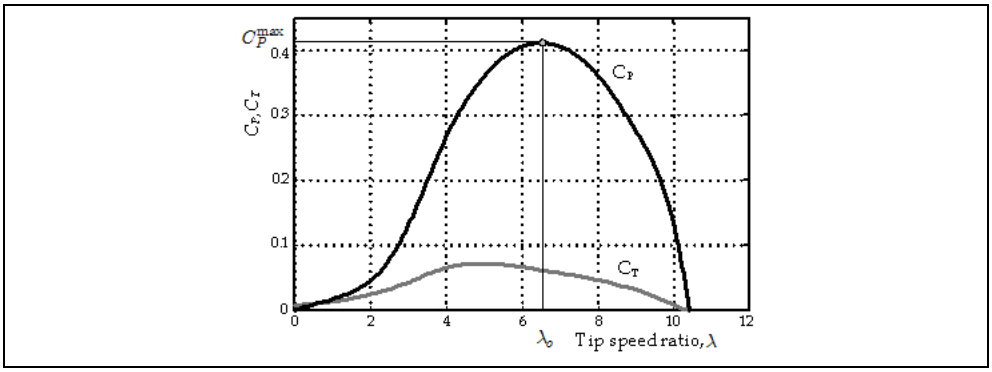

Fig. 1. C_T-λ and C_P- λ characteristics of a typical, 3 kW three blade horizontal wind turbine

2.2 Mathematical model of drive train

The most important part of the drive train is the modeling of the turbine itself as the other parts can be analyzed with common methods. Aerodynamic torque of the turbine is a nonlinear function with respect to the tip speed ratio and the pitch angle. This relation, $C_T(v_t, \omega_t, \beta)$, may be modeled with splines or with look-up tables. The C_T-λ curve is linearized with respect to wind speed, rotational speed, and pitch angle (in the pitch controlled turbine) at a given operating point. To analyze the turbine with linear methods, the non-linear torque function in (5) can be linearized by taking into account only the first terms of the Taylor series (H. Vihriälä, 2002).

$$\Delta T_a = \theta \Delta v_t + \gamma \Delta \omega_t + \kappa \Delta \beta \tag{5}$$

where

$$\theta = \left.\frac{\partial T_a}{\partial v_t}\right|_{O.P.} = C_o \omega_t (2C_{T,o} - \lambda_o \left.\frac{\partial C_T}{\partial v_t}\right)\Big|_{O.P.} \tag{6}$$

$$\gamma = \left.\frac{\partial T_a}{\partial \omega_t}\right|_{O.P.} = C_o R \omega_o \left.\frac{\partial C_T}{\partial \omega_t}\right|_{O.P.} \tag{7}$$

$$\kappa = \left.\frac{\partial T_a}{\partial \beta}\right|_{O.P.} = C_o \left.\frac{\partial C_T}{\partial \beta}\right|_{O.P.} \tag{8}$$

$$C_o = \frac{\rho}{2}\pi R^3 \tag{9}$$

$$\lambda_o = \frac{\omega_{t,o} R}{v_{t,o}} \tag{10}$$

With linearization around an operating point, the product of the derivative of aerodynamic torque and wind speed may be regarded as an external disturbance. If the pitch angle control is adopted as a means of control, the linearized coefficient κ must be calculated. The dynamics of the pitch actuator may be modeled with the first order dynamics. The

derivatives term $\partial T_a / \partial \beta$ can be obtained from blade design calculations or by identification from tests. Since this chapter deals with the fixed pitch configuration, no further discussion will be made on pitch control modeling.

Aerodynamic torque on a wind turbine is a nonlinear function of λ and β. But for the fixed pitch wind turbines, its pitch angle is constant and therefore, the aerodynamic torque depends only on tip speed ratio. Areodynamic torque in (5) can be rewritten as

$$\Delta T_a = \theta \Delta v_t + \gamma \Delta \omega_t \tag{11}$$

The wind power drive train can be modeled as one mass with the assumptions that there is no interaction between the drive train and tower dynamics, and no gravitational force that acts on the blade which causes periodic excitation. The mathematical model of the drive train consists of aerodynamic torque (12), auxiliary torque (13) and rotational acceleration (14).

$$T_a = J_t \dot{\omega}_t + B_t \omega_t + T_g \tag{12}$$

where J_t = inertia of turbine [kg.m²]
B_t = frictional coefficient of turbine [N.s/m²]
T_g = generator torque [N.m]

$$T_{aux} = T_a - B_t \omega_t \tag{13}$$

$$\dot{\omega}_t = \frac{1}{J_t}(T_{aux} - T_g) \tag{14}$$

If T_g is an input and ω_t is an output of the system, (12) and (13) are rearranged to give

$$T_a - T_g = (\dot{\omega}_t J_t + B_t \omega_t) \tag{15}$$

$$T_a = \theta v_t + \gamma \omega_t \tag{16}$$

From (15) and (16) the block diagram can be drawn as in Fig. 2.

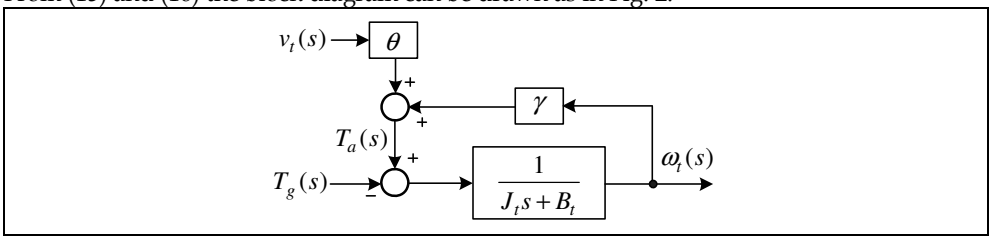

Fig. 2. Block diagram of linearized turbine plant

The closed loop transfer function of the plant is

$$\frac{\omega_t(s)}{T_g(s)} = \frac{1}{(-J_t s - B_t + \gamma)} \tag{17}$$

As the pole of the system is $s = (\gamma - B_t)/J_t$ with $|\gamma| \gg |B_t|$, the sign of the pole depends on the value of γ, which indicates the slope of the C_T-λ curve. This means the system will be unstable if γ is positive (the operating point lies in the left hand side of maximum torque of Fig. 1). Hence, if a linear controller is employed, the controller must be designed to compensate the effect of a positive γ.

2.3 Aerodynamic torque observer

A standard state-space model of a plant can be expressed by (18) and (19).

$$\dot{x} = Ax + Bu \tag{18}$$

$$y = Cx \tag{19}$$

The system can be transformed from the continuous domain to the discrete domain by the z transformation with zero order hold (ZOH), as given in (20) and (21).

$$y[k+1] = \Phi x[k] + \Gamma u[k] \tag{20}$$

$$y[k] = cx[k] \tag{21}$$

The closed-loop observer structure of (22) and (23) is

$$\hat{x}[k+1] = \Phi \hat{x}[k] + \Gamma u[k] + Kc(x[k] - \hat{x}[k]) \tag{22}$$

$$\hat{x}[k+1] = (\Phi - Kc)\hat{x}[k] + \Gamma u[k] + Ky[k] \tag{23}$$

The block diagram with a torque observer in the discrete form is shown in Fig.3. The problem is to calculate the observer gain K of the plant. The mathematical model of the drive train consists of aerodynamic torque (12), auxiliary torque (24) and rotational acceleration (25).

$$T_{aux} = T_a - B_t\omega_t \tag{24}$$

$$\dot{\omega}_t = \frac{1}{J_t}(T_{aux} - T_g) \tag{25}$$

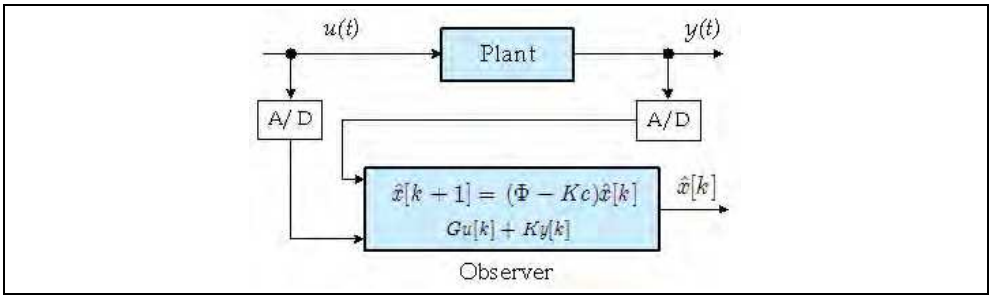

Fig. 3. Block diagram of observer and plant in discrete form

To derive a dynamic torque equation, it is assumed that the aerodynamic torque has much slower variation than a sampling rate, T_s, (Cardenas-Dobson et al., 1996). That is

$$\dot{T}_a = 0 \tag{26}$$

Rearranging (25) and (26) gives

$$\begin{bmatrix} \dot{\omega}_t \\ \dot{T}_{aux} \end{bmatrix} = \begin{bmatrix} 0 & \frac{1}{J_t} \\ 0 & 0 \end{bmatrix} \begin{bmatrix} \omega_t \\ T_{aux} \end{bmatrix} - \begin{bmatrix} \frac{1}{J_t} \\ 0 \end{bmatrix} T_g \tag{27}$$

$$y(t) = [1 \quad 0] \begin{bmatrix} \omega_t \\ T_{aux} \end{bmatrix} \tag{28}$$

From (27) and (28), the observe gain K can be calculated. A mechanical torque observer can then be implemented on a digital signal controller (DSC) board.

3. Control objectives

The wind turbine is an energy converter device that captures energy from the wind and converts it into useful work. Almost all of the wind energy conversion systems are connected to the grid of electric power networks. Although the main objective of wind turbine operation is to optimize energy capture, other technical and environmental objectives should also be satisfied such as mechanical loads, power quality standards, acoustic emission, obstruction, *etc*. (Fernando et al., 2007). These objectives are actually a tradeoff among each other. Thus, the WECS should find a well balanced compromise among them. The control objective of this chapter is emphasized on optimal energy capture.

Due to the requirement in speed control, four wind velocities separate the operation into three operating regions as shown in Fig. 4, which represents a typical power curve of a wind turbine. The cut-in velocity ($v_{cut\text{-}in}$) is defined as the wind speed at which the turbine starts to generate the power. Below this wind speed, it is not efficient to turn on the turbine. The transition speed $v_{\omega N}$ is the wind speed that the operating point starts to move from maximum power curve of region I to the rated power in region III The rated velocity (v_{rated}) is the wind speed at which the turbine reaches its rated turbine power. The cut-out velocity ($v_{cut-out}$) is the maximum wind speed at which the wind turbine can still operate. Beyond this wind speed, the rotor has to be locked to keep the blades, the electrical generator and other components from reaching damage.

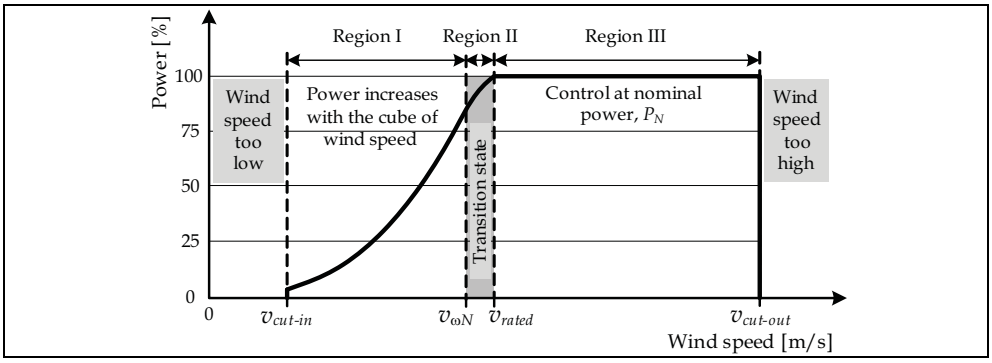

Fig. 4. Operation regions of wind turbine

Region I covers a wind speed range between v_{cut-in} and $v_{\omega N}$ and is referred as the below rated wind speed region. The available power is defined as the power in the wind passing through the rotor area multiplied by the maximum power coefficient $C_P^{\max}$, that is

$$P_{av} = C_P^{\max} P_V = \frac{1}{2}\rho\pi R^3 C_P^{\max} v^3 \tag{29}$$

The control objective in region I is to extract the maximum power from the wind. Therefore, the ideal power curve in this region is a function of wind speed cube defined by (12b). Region II covers a wind speed range between $v_{\omega N}$ and v_{rated} and is referred as a transition between maximum power curve of region I and rated power in region III. In this region, if the rotor speed is so high that it reaches the speed limit, it will generate acoustic noise. Therefore, this region may not exist if the rotor speed is below the limit. Region III covers a wind speed range between v_{rated} and $v_{cut-out}$ and is referred as the above-rated wind speed region. As the mechanical power generated by the rotor is limited, the main task of a controller in this region is to keep output at its rated power (Fernando et al., 2007). Operation regions of interest for wind turbine control of this chapter are those of I and III.

4. Control schemes with variable-speed fixed-pitch wind turbine

As maximum energy conversion is achieved at the fixed optimum angle, keeping the tip speed ratio at λ_o becomes a necessary condition. The constraint $\lambda = \lambda_o$ indicates that the rotor speed must change proportionally to wind speed; to be specific, $\omega_o = \lambda_o v_t / R$. A wind turbine controller uses electronic converters to transfer the output energy from the generator, which produces the counter torque to arrive at ω_o and λ_o, respectively. Thus, the turbine can be controlled to operate at different points, for instance, to track the optimum speed as wind speed fluctuates. The maximum power locus on the torque-speed plane can be obtained from

$$T_o = \frac{1}{2\lambda_o^3}\rho\pi R^5 C_P^{\max}\omega_o^2 = c\omega_o^2 \tag{30}$$

where T_o= optimum torque [N.m]

$$c = \frac{1}{2\lambda_o^3}\rho\pi R^5 C_P^{\max}$$

ω_o= optimum rotational speed [rad/s]

Equation (30) presents a parabola equation between the torque and rotational speed. In below-rated wind speed region, the turbine is controlled to track this $C_P^{\max}$ locus. Thus, variable-speed control strategies essentially differ in the way power is limited in the above-rated wind speed (Munteanu et al., 2008).

This section describes control trajectories to optimize energy capture from the fixed pitch wind turbine in the below-rated and above-rated wind speed regions. Methods to maximize the power output of wind turbines in the below-rated wind speed region are 1) torque reference-based MPPT algorithm, 2) searching-based MPPT algorithm and 3) fuzzy-based MPPT algorithm. These three methods are explained in more detail in next section. In the above-rated wind speed region, there are two methods to limit the output power from the

wind turbine at a specified output: 1) passive stall control and 2) active stall with rotational speed control.

In the below-rated wind speed region, especially, between $v_{cut\text{-}in}$ and v_{rated} (see Fig. 5), the wind turbine is programmed to operate along the quadratic curve AB with the $C_P^{\max}$ path. The turbine is operated at variable speed in this region. In the above-rated wind speed, when the wind speed exceeds the nominal level, the angle of attack will increase and thus approaches stalling. The air stream separates into larminar flow and eddy current flow at some parts of blade profile. Depending upon the angle of attack, the lift force is reduced but the drag force increases. This phenomenon is called passive stall.

Without a mechanism to turn the blades around the axis (i.e., pitch angle is constant), rotational speed control is another method to control the wind turbine to regulate output power in the stall region. For instant, when the controller reduces the rotational speed, the power coefficient will decrease to limit the output power at the nominal value as shown in the path BC of Fig. 5. The wind turbine is operated at variable speed throughout its operational range. If the wind speed approaches to the value at which the nominal power is produced, further torque development at the rotor must be limited. In general, the active stall is more efficient than the passive stall for energy regulation (Erich Hau, 2002).

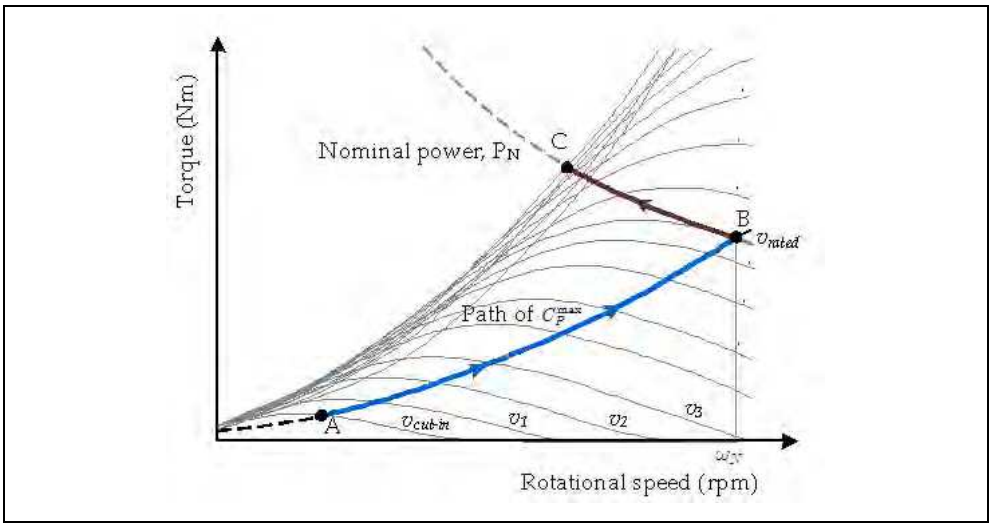

Fig. 5. Active stall with rotational speed control (path BC)

5. Maximum peak power tracking algorithms

The main purpose of MPPT algorithms is to maintain operating points on $C_P^{\max}$ for any wind speeds in the below-rated wind speed region (see Fig. 6). The operating points can be on the positive slope (the left side of $C_P^{\max}$), zero slope (at $C_P^{\max}$), and negative slope (the right side of $C_P^{\max}$). If an operating point is in the positive slope region, the controller will move it to the right towards the optimum tip speed ratio, λ_o. This can be achieved by decreasing load current which results in an increase in the rotational speed. Conversely, if the operating point lies on the right hand side of the peak, the load current has to be

increased, resulting in a decrease in the rotational speed. With this principle, the operating point can be maintained at $C_P^{\max}$ for various wind speeds.

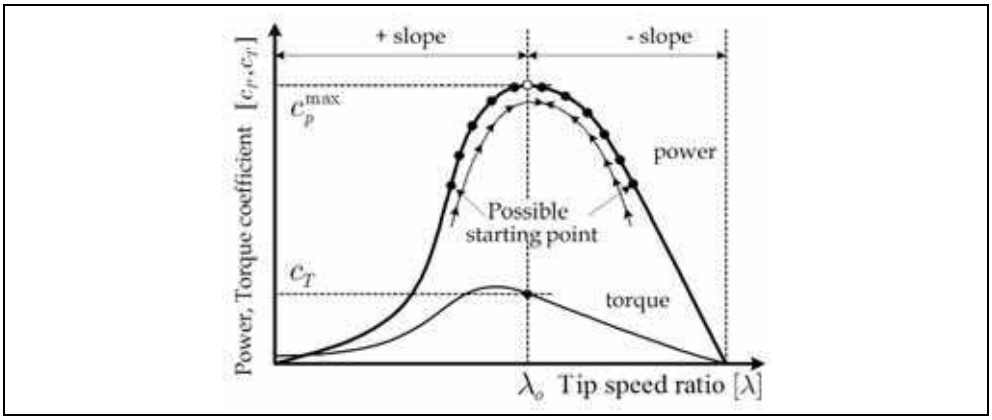

Fig. 6. Power and torque with MPPT tracking process

5.1 Torque reference-based MPPT algorithm

This method requires the wind turbine characteristics (e.g., R, $C_P^{\max}$ and λ_o). The below-rated wind speed reference torque, T_{be}^{ref}, can be calculated by substituting (1) into (4).

$$T_{be}^{ref} = k_t \omega_t^2, \quad P_a < P_{rated} \tag{31}$$

where $k_t = \frac{1}{2}\rho\pi R^3 C_P^{\max}$

λ_o= tip speed ratio at $C_P^{\max}$ [rad.s]

The reference torque for the above-rated wind speed, T_{ab}^{ref}, is calculated from the rated power, P_{rated}.

$$T_{ab}^{ref} = P_{rated} / \omega_t, \quad P_a \geq P_{rated} \tag{32}$$

The controller uses (31) and (32) as the reference torque to control the plant. The torque reference-based MPPT algorithm can be alternatively achieved by testing the wind turbine to find the optimal torque-rotation speed curve with various wind speeds as shown in Fig. 7 a). The reference torque trajectory can be mathematically written as a function of torque and rotational speed or it can be stored as a look-up table which is easy to be programmed in a microcontroller or a DSC board. Figures 7 a) and b) show a reference torque trajectory and the associated output power in the below- and above-rated wind speed regions, respectively (Morimoto et al., 2005).

Control block diagram of torque reference-based MPPT

The torque reference-based MPPT block diagram is shown in Fig. 8. This system receives the rotational speed from the plant. The rotational speed is sent to the torque reference look-up table to interpolate the aerodynamic torque reference, T_{ref}. This reference will be sent to a load regulation loop (lower right corner of the figure), where a proportional-integral (PI) compensator is used to control the load current as desired and improve system stability.

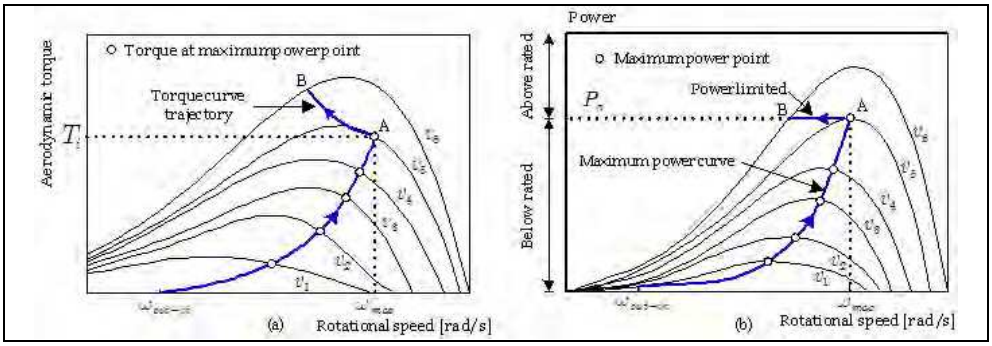

Fig. 7. a) Optimum torque trajectory and b) optimal power trajectory

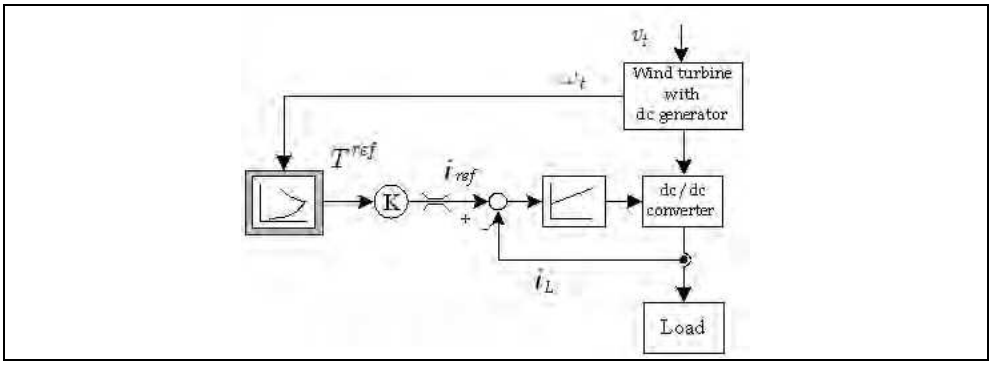

Fig. 8. Control block diagram of torque reference-based MPPT

5.2 Searching-based MPPT algorithm

This algorithm brings the operating point toward $C_p^{\max}$ by increasing or decreasing the rotational speed step by step. This tracking methodology is called the perturbation and observation method. To limit the output power at a specified power limit by stall regulation, the controller will reduce the rotational speed until the power coefficient reduces to the power limit. If the output is lower than the power limit, the controller will increase the rotational speed until the power matches the power limit. The control flowchart of the maximum power tracking system in Fig. 9 illustrates the details of decision processes based on the tracking procedure in Fig. 7. If the rotational speed is higher than the cut-in speed, $\omega_{cut\text{-}in}$, the MPPT controller will start the procedure. If a given perturbation leads to a positive or negative slope, the next perturbation increases or decreases the rotational speed until the slope becomes zero (i.e., maximum power point is reached). An updated load current reference, i_{ref}, for each sampling period, T_s, and an instantaneous power slope are calculated by (33) and (34), respectively (Morimoto et al., 2005) and (A.M De Broe et al., 1999).

$$i_{ref}[(k+1)T_s] = i_{ref}[kT_s] + M\frac{\Delta p[(k)T_s]}{\Delta\omega_t[(k)T_s]} \tag{33}$$

$$slope = \frac{\Delta p[(k)T_s]}{\Delta \omega_t[(k)T_s]} \tag{34}$$

where M = updated factor [-]
$i_{ref}[kT_s]$ = current at kT_s [A]

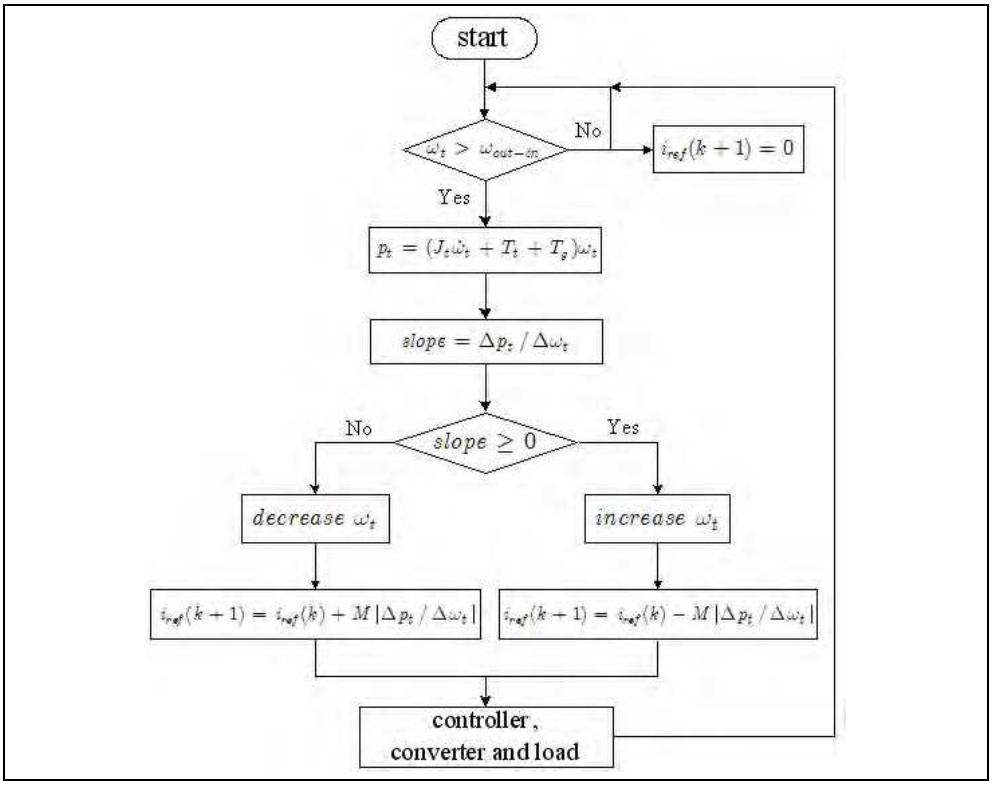

Fig. 9. Searching-base MPPT algorithm flowchart

Control block diagram of searching-based MPPT

To implement the MPPT and stall regulation control in a DSC controller unit, the total power *Pt* should be written in more detail as given in (35).

$$P_t = J_\omega \dot{\omega}_t \omega_t + P_e + T_f \omega_t + V_b i_g + i_g^2 R_g \tag{35}$$

The overall block diagram of MPPT and stall regulation control system is shown in Fig. 10. The top part of the diagram which is enclosed in the dotted line represents the MPPT controller built from (35) for the below-rated wind speed region. The below-rated wind speed control receives the generator current, voltage and rotational speed from the plant as inputs and use them to calculate the slope of the power-speed curve. The rate of change of power is compared with the reference (zero rate of change of power). The error is multiplied by a dc gain to generate the current reference for the PI controller of the plant control system. The lower part of the block diagram in Fig. 10, which is enclosed by the dotted line,

represents the stall control for power limit. This controller receives the magnitude of the total power value from the below-rated control block diagram. If the instantaneous power is greater than the rated power, the selecting switch will be changed to the lower pole. This PI compensator in the load regulation loop (lower right hand corner of the figure) keep the output power within the rated power value.

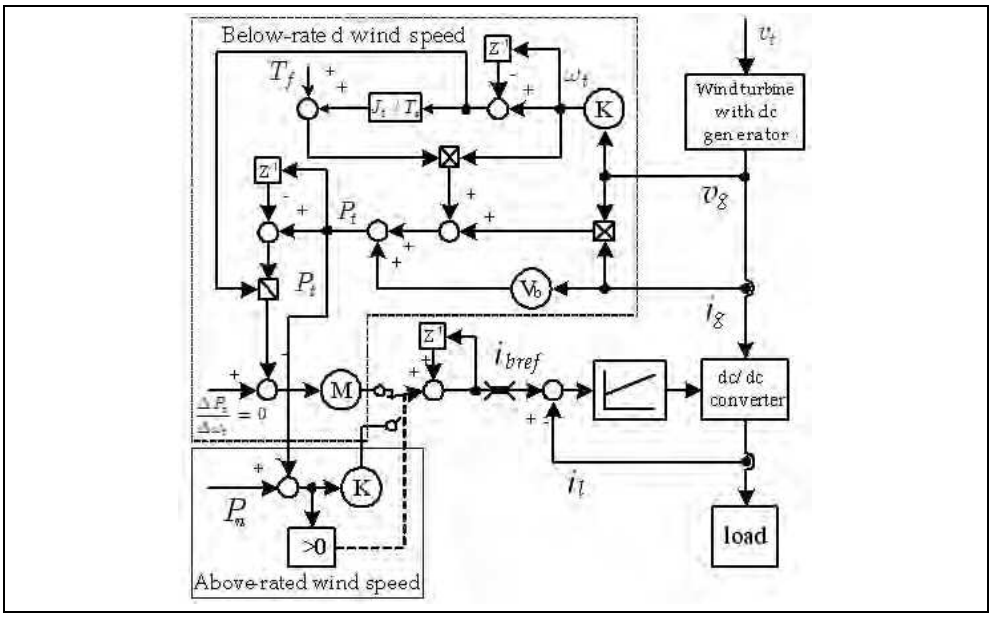

Fig. 10. Block diagram of searching-based MPPT

5.3 Fuzzy-based MPPT algorithm

A fuzzy logic control (FLC) algorithm is characterized by "IF-THEN" rules. The algorithm is suitable for wind turbine control with complex nonlinear models and parameters variation. Like the second algorithm, the fuzzy-based MPPT uses the perturbation and observation to track the maximum output power in the below-rated wind speed without knowledge of wind turbine characteristic. The input variables of the fuzzy-based MPPT are the rotational speed and the aerodynamic torque observer $\hat{T}_a$. In the above-rated wind speed, the FLC uses a torque reference calculated from (6) to limit the output power at the power limit. Another two input parameters, $\Delta\hat{T}_a$ and $\Delta\omega_t$, are used to limit torque and speed fluctuation. The MPPT with FLC uses $\hat{T}_a$ to classify the operating regions.

5.3.1 Fuzzy logic control design for fixed pitch wind turbine

In the below-rated wind speed region, the main control objective is to maximize energy capture from the wind. The wind turbine characteristics has a single maximum power coefficient, $C_P^{\max}$, at the tip speed ratio λ_o. When the rotor operates at constant speed, the power coefficient will be at maximum at only one wind speed and therefore to achieve the highest annual energy capture, the value of the power coefficient must be maintained at the

maximum level all the time (Yaoqin et al., 2002). In order to meet this objective, the controller calculates the reference torque using (36) and uses the error between this reference torque and feedback aerodynamic torque as the main input feedback.

$$T_{be}^{ref} = \frac{\rho}{2}\pi R^5 C_P^{\max}\frac{1}{\lambda_o^3}\omega_t^2 = k_T\omega_t^2 \tag{36}$$

where $k_T = \frac{\rho}{2}\pi R^5 C_P^{\max}\frac{1}{\lambda_o^3}$

The FLC based operation in this region can be explained by the below-rated torque control path in Fig. 11 a). Initially, it is assumed that the operating point is at point a, which corresponds to $C_P^{\max}$ operating point for a wind speed of 6 m/s. If the wind speed reduces to 4 m/s, the operating point will move to b with the same rotational speed, ω_1. For that wind speed, the FLC moves the operating point from b to c, which is the optimal position for the 4 m/s wind speed, by increasing the generator torque to reduce the rotational speed to ω_2. If the wind speed immediately increases from 4 m/s to 6 m/s, the operating point will move up to d, where the power is not maximum. Hence, the FLC will have to move the operating point to point a by reducing the generator torque and therefore increases the rotational speed. The control law for this region is summarized below:

$$\text{If } T_a > T_{be}^{ref}\text{, reduce } \Delta T_g \text{ to increase } \omega \tag{37}$$

$$\text{If } T_a < T_{be}^{ref}\text{, increase } \Delta T_g \text{ to reduce } \omega \tag{38}$$

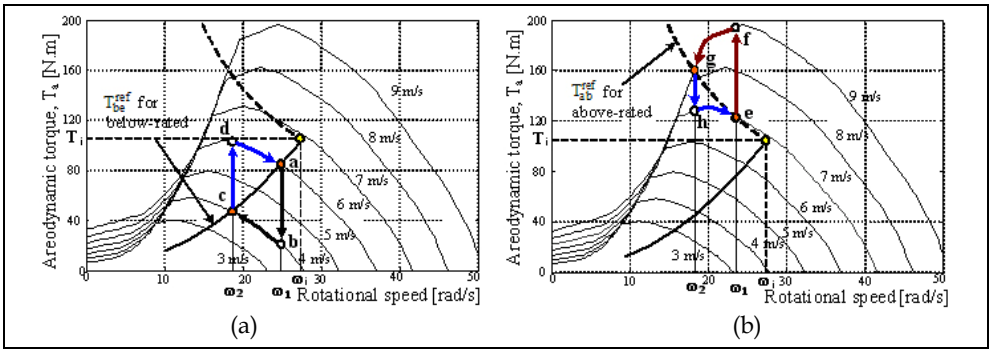

Fig. 11. a) Torque control path in below-rated wind speed region b) Torque control path in above-rated wind speed region

In the above-rated wind speed region, the main control objective is to limit the energy capture at a specified value. Typical methods are pitch control, active stall regulation, and passive stall (Muljadi et al., 1998). For a fixed pitched wind turbine, the active stall with rotational speed control is of interest. The output power can be limited by controlling its tip speed ratio until it is stalled. The controller can limit the output power by reducing the power coefficient, which can be done by moving the operating point to the left or right of ($\lambda_o, C_P^{\max}$). The controller will keep the operating point in the left side of (λ_o, $C_P^{\max}$) to avoid

the system operating in higher rotational speeds. The controller calculates the reference torque based on (39) and can be shown by the dash line in Fig. 11 b). The controller uses the error between the reference and aerodynamic torques as the main input feedback.

$$T_{ab}^{ref} = \frac{P_{rated}}{\omega_t} \tag{39}$$

The intersection of the two regions gives the coordinate ($\omega_{\max}$,T_i), where

$$\omega_{\max} = \sqrt[3]{P_{rated} / k_T} \quad \text{and} \quad T_i = k_T^{1/3} P_{\max}^{2/3} \tag{40}$$

In Fig.11 b), the operating point is assumed to be at point e when the wind speed is 7 m/s. If the wind speed jumps to 9 m/s, the aerodynamic torque will increase accordingly, forcing the operating point to move to f. The FLC will increase the generator torque to reduce the rotational speed. The operating point will then come to a new optimum position, g. Conversely, if the wind speed reduces to 7 m/s, a transition from g to h can be expected. Thus the FLC will reduce the generator torque to increase the rotational speed to move the operating point to e, based on the reference torque path. The control law for this region is

$$\text{If } T_a > T_{ab}^{ref} \text{, increase } \Delta T_g \text{ to reduce } \omega \tag{41}$$

$$\text{If } T_a < T_{ab}^{ref} \text{, reduce } \Delta T_g \text{ to increase } \omega \tag{42}$$

Note that other constrains to be taken into account for the fuzzy logic control are, for example, changes in the rotational speed and torque.

5.3.2 Fuzzy logic control

In the fuzzification process, the relevant numerical parameters are linguistically converted into equal-base symmetric triangles (for the output) and trapezoidal membership functions (Bimal, 2000). The membership functions for six input parameters consisting of E_{be} and E_{ab}, defined in (43), Figure 12 shows the membership functions of 6 variables, namely E_{be}, E_{ab}, T_a, ΔT_a, ω_t, and $\Delta\omega_t$. The aerodynamic torque observer described in section 3.2 is used to observe aerodynamic torque, $\hat{T}_a$, in order to construct four inputs E_{be}, E_{ab}, T_a, and ΔT_a. The rotational speed ω_t is measured by 1000-pulse rotary encoder to obtain the rotational speed and the change of rotational speed $\Delta\omega_t$ as the other inputs of FLC. The membership function for one output parameter, ΔT_g, is shown in Fig. 13. All the membership functions are normalized in a range of [-1,1].

$$E_{be} = T_{be}^{ref} - T_a \quad \text{and} \quad E_{ab} = T_{ab}^{ref} - T_a \tag{43}$$

The fuzzy rule base that associates the fuzzy output to the fuzzy inputs is derived from the system behavior. It basically contains the knowledge acquired by designers as fuzzy rules and is expressed in forms of IF-THEN rules. The sole objective of the fuzzy rules designed here is to keep the wind turbine operating at the optimal point by using torque control for the two regions (Simoes et al., 1997).

In the below-rated wind speed region, the FLC knows how to operate in this region by observing whether the aerodynamic torque is lower than T_i (40). In this region, only three

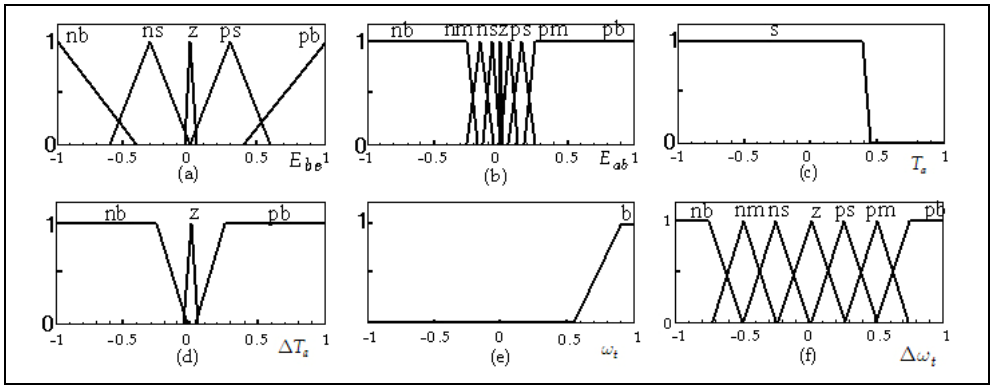

Fig. 12. Membership function input variables of a) E_{be}, b) E_{ab}, c) T_a, d) ΔT_a, e) ω_t, f) $\Delta\omega_t$

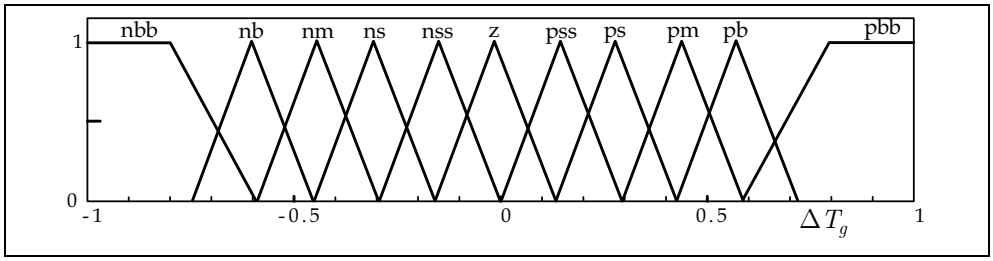

Fig. 13. Membership function output variables ΔT_g
where

nbb = negative big big		nb = negative big		nm = negative medium	
ns = negative small		nss = negative small small		z = zero	
pss = positive small small		ps = positive small		pm = positive medium	
pb = positive big		pbb = positive big		b = big	
s = small					

input parameters are needed to determine the output: T_a, $\Delta\omega_t$ and E_{be}. The FLC tracks the torque reference given in (36) to obtain the maximum peak power. The relationship between $\Delta\omega_t$ and E_{be} generates ΔT_g with 35 rule base when T_a is s (see Fig. 12 c).
In the above-rated wind speed region, when the aerodynamic torque is grater than T_i (i.e., T_a is ns), the FLC tracks the torque reference by (39) and uses five input parameters, E_{ab}, $\Delta\omega_t$, ΔT_a, T_a and ω_t , to generate ΔT_g. The first three parameters are used to create the 105 rule base whereas T_a decides in which region the controller will operate. The final parameter is used for over-speed protection; to be specific, if ω_t is b, then ΔT_g is pbb.
Defuzzification is a process that converts the fuzzy set representing the overall conclusion into a real number after the evaluation of the rule base module. There are various types of defuzzification but a widely used one is the center of gravity (or centroid) defuzzification method, which determines the center of gravity of output membership function. If the discrete fuzzy set is applied in Fig. 14, the center of gravity of output membership function can be obtained from (Simoes et al., 1997)

$$U_0 = \sum_{i=1}^{n} U_i \mu(U_i) / \sum_{i=1}^{n} \mu(U_i) \tag{44}$$

where U_i = area of final fuzzy value at i
$\mu(U_i)$ = fuzzy output value i

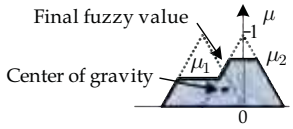

Fig. 14. Discrete fuzzy defuzzification for center of gravity method

5.3.3 Fuzzy logic control block diagram

The FLC block diagram of the system is shown in Fig. 15 (Neammanee et al., 2006). This system receives the current, voltage and rotational speed from the plant and then sends them to the torque observer to estimate the aerodynamic torque, $\hat{T}_a$. The FLC calculates ΔT_g using the predefined membership functions, fuzzy rule base and defuzzification to update the output torque and output command (Neammanee et al., 2007).

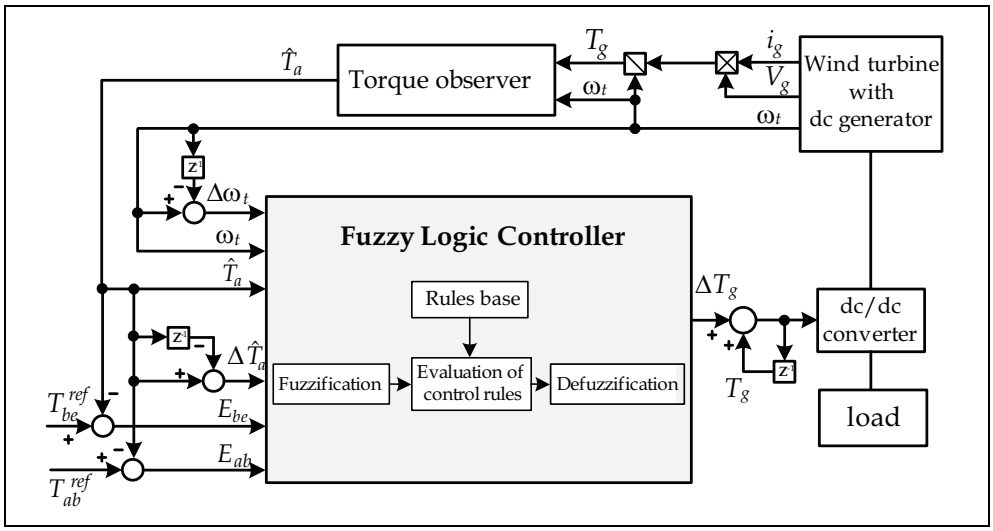

Fig. 15. Block diagram of fuzzy logic controller wind turbine

6. Case studies

The test system is composed of two main parts: 1) a developed wind turbine simulator on the left side of Fig. 16. and 2) a purposed wind turbine controller on the right side. The wind turbine simulator consists of a torque control inverter connected to a 7.5 kW induction motor and voltage and current sensors, data acquisition and a DSC controller board. The

DSC controller board uses a high performance 16 bits dsPIC30f6010, which combines the advantage of a high performance microcontroller and high computation speed digital signal processors (Huynh, P. & Cho, B.H., 1996). The software used to control the simulator was implemented in this DSC linked with a personal computer via two RS232 ports: one for transferring wind speed data to the DSC board and the other for sending parameters (e.g., P_e , i_g, v_g, ω_g) to the computer. The proposed wind turbine controller on which the MPPT algorithms are implemented consists of a dc/dc converter connected between a generator and a load, voltage and current sensors, a data acquisition unit and a DSC controller with the same performance as the one used in the simulator (Neammanee et al., 2007).

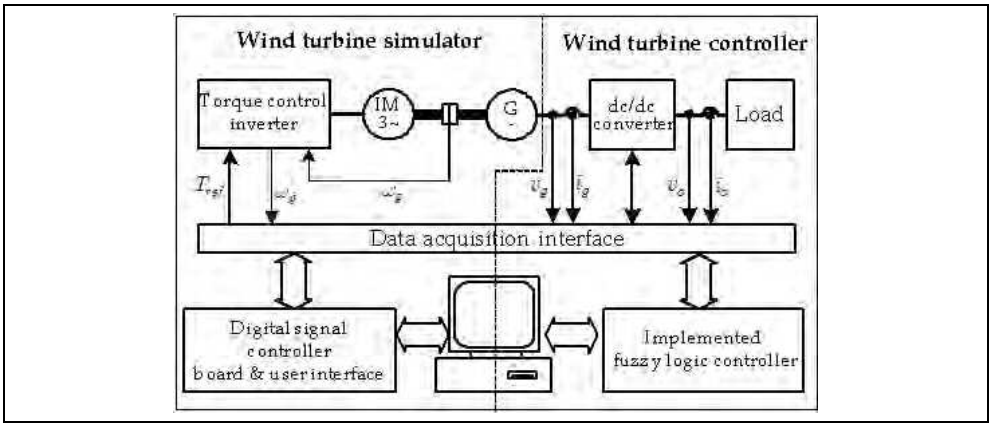

Fig. 16. Test system

6.1 MPPT algorithm and active stall regulation with rotational speed control

Figures 17-19 show control trajectories of the three MPPT-based algorithms with five different wind speeds: 3, 3.5, 4, 4.5 and 5 m/s. As can be seen from the figures, in the below-rated wind speed (less than 700W), the MPPT with torque reference controller succeeds in tracking the maximum power for each wind speed with the lowest rotational speed variation. When the wind speed is stepped up from 4.5 to 5 m/s, the system starts to limit the output power at 700W. If the wind speed increases beyond 5 m/s, the operating point will move to the left hand side of the previous one with a constant output power of 700W but with higher aerodynamic torques. During the move, the controller decreases the rotational speed until the wind turbine has been stalled. It can be seen that there is a high fluctuation in the output power in the above-rated wind speed.

The searching-based MPPT controller tracks the maximum peak power at each wind speed with highest rotational speed fluctuation in the below-rated wind speed. Around the output power limit (700 W), it is observed that this algorithm has a slightly lower power fluctuation than that of the first algorithm. Note that the second algorithm uses the lower part of the control diagram in Fig. 8 to calculate the reference torque in the above-rated wind speed. Referring to Fig. 15, the fuzzy based MPPT controller tracks the maximum peak power with the lowest power fluctuation as well as fairly low rotational speed fluctuation in the below-rated wind speed. The tracking time for the three control algorithms is compared in Fig. 20. It is clearly seen that the torque reference-based MPPT and the fuzzy-based MPPT are

fastest in the below-rated wind speed and the above-rated wind speed, respectively (Neammanee et al., 2008).

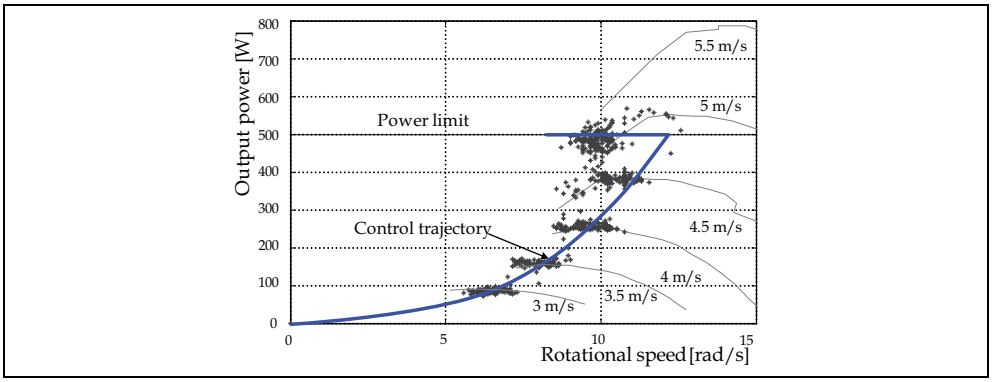

Fig. 17. Control trajectory of torque reference-based MPPT algorithm

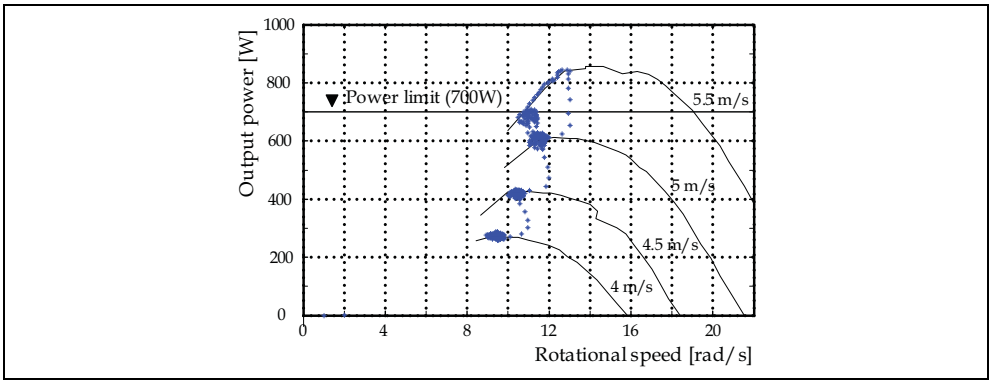

Fig. 18. Control trajectory of searching-based MPPT searching algorithm

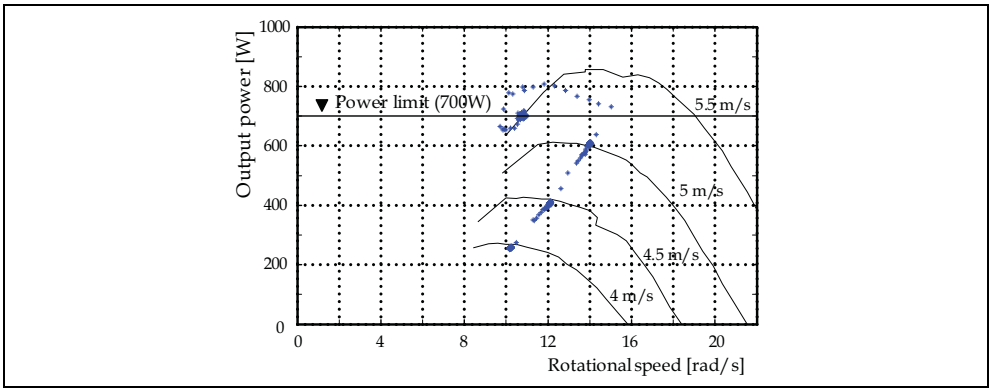

Fig. 19. Control trajectory of fuzzy-based MPPT algorithm

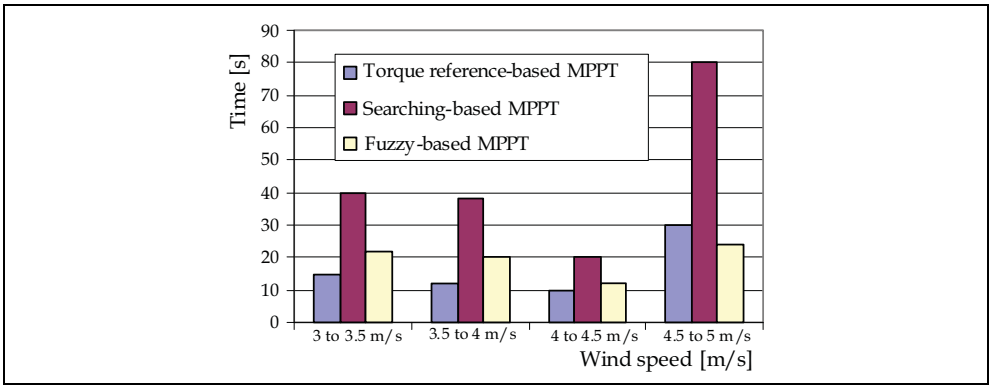

Fig. 20. Tracking time of three algorithms

6.2 MPPT algorithm with grid connected converter

There are three main parts of the test system shown in Fig. 21: 1) a 7.5 kW wind turbine simulator source on the left hand side of the figure, 2) a purposed MPPT controller with a high performance double-interleaved dual boost converter for the wind turbine in the middle, and 3) a 3 kW single phase grid connected converter on the right side. The wind turbine simulator is used to test the searching-based MPPT with the double-interleaved dual boost converter.

The purpose of this experiment is to confirm that the MPPT controller can be used with the DIDB converter to maximize power. This experiment was tested with various input wind speeds to the wind turbine simulator, coupled to a dc generator connected to the grid via the DIDB converter. The wind simulator was started at a wind speed of 4m/s, stepped up to 4.5, 5, 5.5 and 6 m/s respectively and run until steady state. The MPPT controller would capture a maximum power of 260, 380, 580, 700 and 900 W respectively. Figure 23 a) shows the relationship between the output power and time with various wind speeds. It can be seen from Fig. 23 b) that in this case, the MPPT controller can manage to keep C_P at the optimum

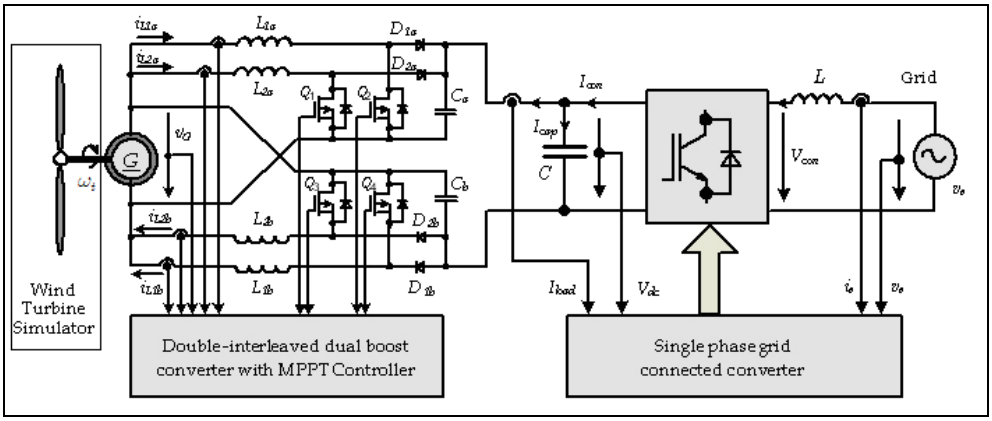

Fig. 21. Schematic diagram of test system

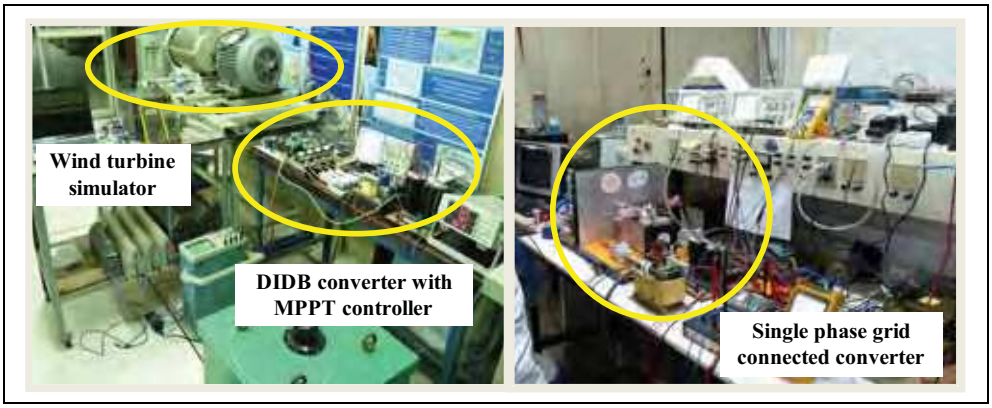

Fig. 22. Hardware of test system

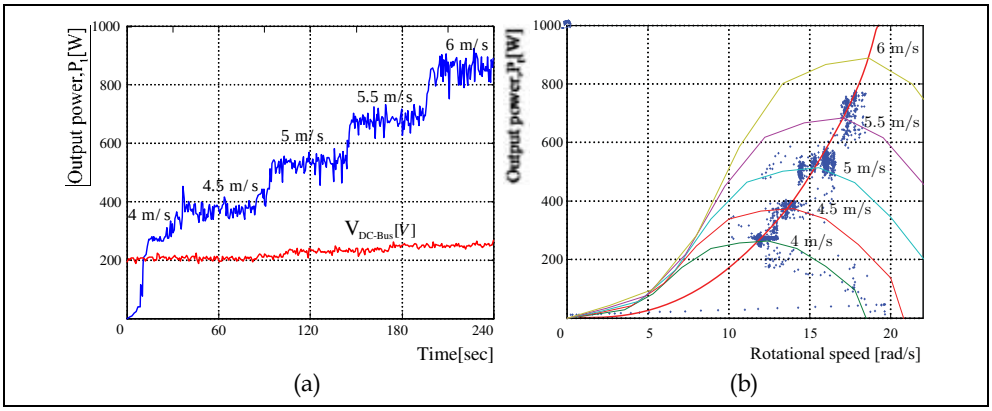

Fig. 23. a) 2-kW DIDB converter with MPPT controller b) Control trajectory of MPPT controller with various wind speeds

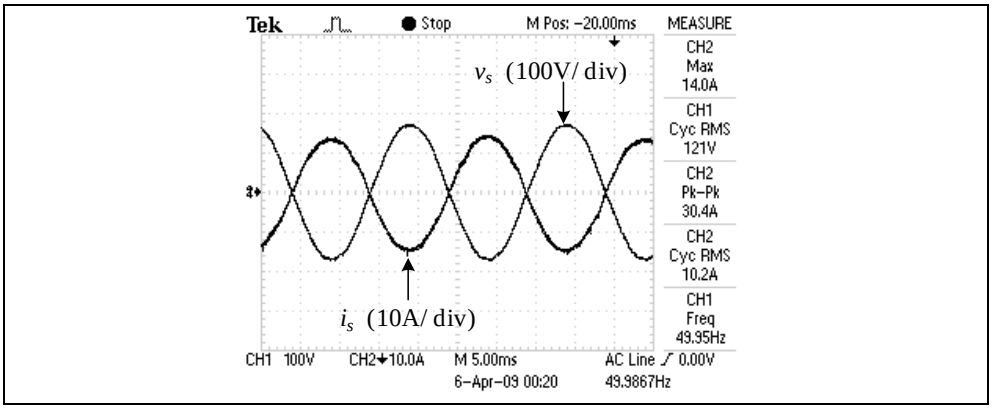

Fig. 24. Line voltage, v_s and current, i_s , measured by oscilloscope

value (λ_o) for the 5 step wind speeds. This experiment also reveals that the DIDB converter and the MPPT controller can be combined to achieve maximum power tracking. Figure 24 shows the phase voltage v_s and current i_s measured by oscilloscope on the grid side in inverting mode under steady state operation. It is clearly seen that phase current has a low total harmonic distortion. The phase voltage and current are 180° out of phase, indicating this converter generates only active power to the grid. The output power and dc bus voltage for real wind speed input data, v_t, to the wind turbine simulator are shown in Fig. 25. It is clear that the MPPT controller can track the maximum (Kajangpan et al., 2009).

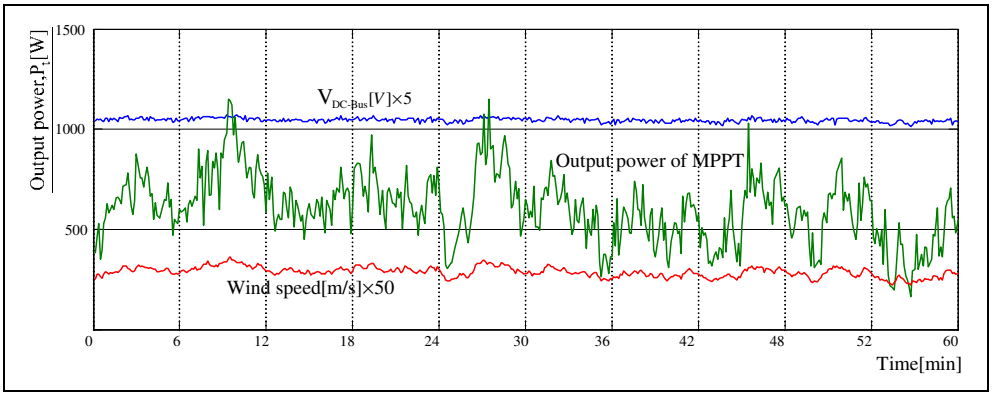

Fig. 25. Wind speed, output power of MPPT and dc-link voltage

7. Conclusion

This chapter is emphasized on control strategies for a variable speed fixed-pitch wind turbine with the main objective to optimize energy capture in below- and above-rated wind speed regions. Two main laboratory experiments were conducted: 1) three maximum peak power tracking (MPPT) algorithms and active stall regulation with rotational speed control, and 2) an MPPT algorithm with a grid-connected converter. All the MPPT algorithms were implemented on a low cost DSC board and tested with a developed wind turbine simulator. The first algorithm tracks the maximum power using a torque reference obtained from the wind turbine characteristic. The second method is based on the observation that the power versus rotational speed curve has a single well defined peak. Therefore, a necessary condition for the speed being at the maximum power point is that the first derivative of the power respect to the rotational speed is zero. The third algorithm employs a fuzzy logic as the key controller.

It can be concluded from the first experimental results that the MPPT with torque reference offers fastest tracking time in the below-rated wind speed region and the MPPT with fuzzy logic is favored in terms of power fluctuation and tracking time in the above-rated wind speed region. Although the second MPPT algorithm has the slowest tracking time and the highest rotational speed fluctuation, it is attractive for a small amount of computational resource and therefore low cost for implementation. Although the FLC possesses many advantages as described above, the implementation of the FLC is quite complicated,

especially in the software part. For example, the implementation of the FLC with 140 rule base requires 1) plant knowledge to construct the rule base, 2) simulation process before implementation and 3) large memory storage for control program.
The second experimental results confirm that a developed grid connected converter with an MPPT algorithm can deliver the output power with low input current ripple and high gain. The system can track the maximum output power with step and various wind speeds and can regulate the dc bus voltage with nearly sinusoidal line side current, near-unity power factor and low harmonic distortion.
The proposed methodology can be extended to develop an adaptive FLC algorithm by the knowledge-base system for data recording in intelligent updated memory (IUM) to reduce the generator current and recording time. By applying the MPPT controller in the initial mode of tracking, the maximum power operating points can be located. These data will be stored in an IUM. When the data in the IUM cover a specified range in the below-rated wind speed region, the adaptive FLC will use these data as an input to maximize the output power within the range. The adaptive FLC, which consists of a MPPT controller, a torque observer, an IUM recorder and a FLC, can be implemented on a low cost, high performance digital signal controller board with a microcomputer for data acquisition and control verification.

8. Acknowledgement

The authors would like to express sincere thank to Energy Policy and Planning Office, Ministry of Energy, Thailand, and Faculty of Engineering, King Mongkut's University of Technology North Bangkok (KMUTNB) for financial supports.

9. References

A. Mirecki, X. Roboam, F. Richardeau (2004). Comparative Study of Maximum Power Strategy in Wind Turbines, *IEEE Trans. Ind. Electronics*. Vol. 2, 4-7 May., pp. 993-998.

A.M De Broe, S.Drouilhet, V. Gevorgian (1999). A Peak Power Tracker for Small Wind Turbines in Battery Charging Applications, *IEEE Transactions on Energy Conversion*, Vol. 14, No. 4, Dec., pp. 1630-1635.

B. Neammanee, K. Krajangpan S. Sirisumrannukul and S.Chatratana (2006). Fuzzy Logic Based Optimal Energy Capture for Wind Energy Conversion Systems, *The 10 Conference of the Electrical Power Supply Industry (CEPSI),* Mumbai, India.

B. Neammanee, S. Sirisumranukul, S. Chatratana (2007). Development of a Wind Turbine Simulator for Wind Generator Testing. *International Energy Journal*. pp. 21-28.

B. Neammanee, K. Krajangpan, S. Sirisumrannukul and S. Chatratana (2008), Maximum Peak Power Tracking-Based Control Algorithms with Stall Regulation for Optimal Wind Energy Capture, the industry applications transaction, *The Institute of Electrical Engineering of Japan (IEEJ)*, Vol. 128, No.4, Japan, 1 Apr., pp.: 411-417.

Bimal K. Bose (2000). Fuzzy Logic and Neural Networks, *IEE Inds. App. Magazine*, May/June. pp.57-63.

E. Muljadi, K. Pierce and P. Migliore (1998). Control Strategy for Variable-Speed, Stall-Regulated Wind Turbines, American Control con. Pennsylvania, USA, June, pp. 1710-1714.

Erich Hau (2002). *Wind turbines*. Spring-Verlag, ISBN-10 3-540-24240-6, Berlin Heidelberg.

Fernando, D. Bianchi; Hernan De Battista & Ricardo, J. Mantz. (2007). *Wind Turbine Control Systems,* Springer-Verlag, ISBN-13:9781846284922, London.

H. Vihriälä (2002). *Control of Variable Speed Wind Turbine*. Ph.D. Thesis. Tampere University of Technology.

H.M. Kojabadi, Liuchen Chang, T. Boutot (2004). Development of a Novel Wind Turbine Simulator for Wind Energy Conversion Systems Using an Inverter-Controlled Induction Motor, *Energy Conversion IEEE Tran.* on Vol. 19, Issue 3, Sep., pp. 547-552.

Huynh, P. and Cho, B.H. (1996). Design and analysis of a Microprocessor-Controlled Peak-power-Tracking System, *Aerospace and Electronic Systems, IEEE Tran.* Vol. 32, Issue 1, Jan., pp.182 -190.

Iulian Munteanu; Antoneta Iuliana Bratcu, Nicolaos-Antonio Cutululis ; Emil Ceanga (2008). *Optimal Control of Wind Energy Systems,* Springer-Verlag, ISBN-978-1-84800-080-3, London.

Jia Yaoqin, Yang Zhongqing, Cao Binggang (2002). A New Maximum Power Point Tracking Control Scheme for Wind Generation, *IEEE Con. on Power System Technology*, Vol. 1, 13-17 Oct. pp.: 144-148.

Korawit Kajangpan, Bunlung Neammanee and Somporn Sirisumranukul (2009). High Performance Grid Connected Converter with Double-Interleaved Dual Boost Technique and MPPT Control for Wind Turbine," *World Renewable Energy Congress 2009 – Asia, The 3rd International Conference on "Sustainable Energy and Environment (SEE 2009)*" Bangkok, Thailand, 18-23 May, pp.: 718-722.

Morimoto, S.; Nakayama, H. Sanada, M.; Takeda, Y.(2005). Sensorless Output Maximization Control for Variable-Speed Wind Generation System Using IPMSG, *Ind. Appl., IEEE Trans*, Vol. 41, Issue 1, Jan.-Feb. pp.:60- 67.

Morimoto, S.; Nakayama, H. Sanada, M.; Takeda, Y.; (2005). Sensorless Output Maximization Control for Variable-Speed Wind Generation System Using IPMSG. Ind. Appl., IEEE Trans Vol. 41, Issue 1, Jan.-Feb. pp.:60- 67.

Marcelo Godoy Simoes, Bimal K. Bose, Ronald J. Spiegel, (1997). "Design and Performance Evaluation of a Fuzzy-Logic-Based Variable-Speed Wind Generation System." *Industrial Application IEEE Trans.* on Vol. 33 No. 4 (Jul./Aug.,) pp. 956-965.

Marcelo Godoy Simoes, Bimal K. Bose and Ronald J. Spiegel, (1997). Design and Performance Evaluation of a Fuzzy-Logic-Based Variable-Speed Wind Generation System. *Industrial Application IEEE Trans*. on Vol. 33 No. 4 (Jul./Aug.,) pp. 956-965.

R. Cardenas-Dobson, G.M. Asher and G. Asher (1996). Torque Observer for the Control of Variable Speed Wind Turbines Operating Below Rated Wind Speed, *Wind Engineering*, Vol. 20, No.4, pp. 259-285.

Wind Power

Edited by S M Muyeen

ISBN 978-953-7619-81-7
Hard cover, 558 pages
Publisher InTech
Published online 01, June, 2010
Published in print edition June, 2010

This book is the result of inspirations and contributions from many researchers of different fields. A wide verity of research results are merged together to make this book useful for students and researchers who will take contribution for further development of the existing technology. I hope you will enjoy the book, so that my effort to bringing it together for you will be successful. In my capacity, as the Editor of this book, I would like to thanks and appreciate the chapter authors, who ensured the quality of the material as well as submitting their best works. Most of the results presented in to the book have already been published on international journals and appreciated in many international conferences.

How to reference

In order to correctly reference this scholarly work, feel free to copy and paste the following:

Bunlung Neammanee, Somporn Sirisumrannukul and Somchai Chatratana (2010). Control Strategies for Variable-speed Fixed-pitch Wind Turbines, Wind Power, S M Muyeen (Ed.), ISBN: 978-953-7619-81-7, InTech, Available from: http://www.intechopen.com/books/wind-power/control-strategies-for-variable-speed-fixed-pitch-wind-turbines

INTECH
open science | open minds

InTech Europe
University Campus STeP Ri
Slavka Krautzeka 83/A
51000 Rijeka, Croatia
Phone: +385 (51) 770 447
Fax: +385 (51) 686 166
www.intechopen.com

InTech China
Unit 405, Office Block, Hotel Equatorial Shanghai
No.65, Yan An Road (West), Shanghai, 200040, China
中国上海市延安西路65号上海国际贵都大饭店办公楼405单元
Phone: +86-21-62489820
Fax: +86-21-62489821